the OH Radical and Chlorine Atom Kinetics of Substituted Aromatic Compounds: 4-chlorobenzotrifluoride (para-ClC6H4CF3)

Aparajeo Chattopadhyay, Yuri Bedjanian, Manolis Romanias, Angeliki Eleftheriou, Vasilios Melissas, Vassileios Papadimitriou, James Burkholder

The OH Radical and Cl Atom Kinetics of Substituted Aromatic Compounds: 4-chlorobenzotrifluoride (para-$ClC_6H_4CF_3$)

Aparajeo Chattopadhyay,[1,2] Yuri Bedjanian,[3] Manolis N. Romanias,[4] Angeliki D. Eleftheriou,[5] Vasilios S. Melissas,[6] Vassileios C. Papadimitriou,[1,2,5 *] and James B. Burkholder[1 *]

[1] Chemical Sciences Laboratory, National Oceanic and Atmospheric Administration, 325 Broadway, Boulder, CO, USA 80305-3327
[2] Cooperative Institute for Research in Environmental Sciences, University of Colorado, Boulder, CO, USA 80309
[3] Institut de Combustion, Aérothermique, Réactivité et Environnement (ICARE), CNRS 45071 Orléans Cedex 2, France
[4] Institut Mines-Télécom Nord Europe, Univ. Lille, Center for Energy and Environment, F-59000 Lille, France
[5] Laboratory of Photochemistry and Chemical Kinetics, Department of Chemistry, University of Crete, Vassilika Vouton, 70013, Heraklion, Crete, Greece
[6] Department of Chemistry, University of Ioannina, Ioannina GR-45110, Greece

* Corresponding authors:
Vassileios C. Papadimitriou
Laboratory of Photochemistry and Chemical Kinetics,
Department of Chemistry, University of Crete,
Vassilika Vouton, 70013, Heraklion, Crete, Greece
Ph: +30 2810 5450 93
Email: bpapadim@uoc.gr
ORCID: 0000-0002-8299-4306

James B. Burkholder
Chemical Sciences Laboratory,
National Oceanic and Atmospheric Administration,
325 Broadway, Boulder, CO 80305-3328.
Ph: 303-351-2739
Email: James.B.Burkholder@noaa.gov
ORCID: 0000-0001-9532-6246

Abstract

The mechanisms for the OH radical and Cl-atom gas-phase reaction kinetics of substituted aromatic compounds remains a topic of atmospheric and combustion chemistry research. 4-chlorobenzotrifluoride (para-chlorobenzotrifluoride, *p*-$ClC_6H_4CF_3$, PCBTF) is a commonly used substituted aromatic volatile organic compound (VOC) in solvent-based coatings. As such, PCBTF is classified as a volatile chemical product (VCP) whose release into the atmosphere potentially impacts air quality. In this study, rate coefficients, k_1, for the OH + PCBTF reaction were measured over the temperature ranges 275–340 K and 385–940 K using low-pressure discharge flow-tube reactors coupled with a mass spectrometer detector in the ICARE/CNRS (Orléans, France) laboratory. k_1(298–353 K) was also measured using a relative rate method in the thermally regulated atmospheric simulation chamber (THALAMOS; Douai, France). k_1(T) displayed a non-Arrhenius temperature dependence with a negative temperature dependence between 275 and 385 K given by $k_1(275–385\ K) = (1.50 \pm 0.15) \times 10^{-14} \exp((705 \pm 30)/T)$ cm^3 $molecule^{-1}$ s^{-1}, where $k_1(298\ K) = (1.63 \pm 0.03) \times 10^{-13}$ cm^3 $molecule^{-1}$ s^{-1} and a positive temperature dependence at elevated temperatures given by $k_1(470–950\ K) = (5.42 \pm 0.40) \times 10^{-12} \exp(-(2507 \pm 45)/T)$ cm^3 $molecule^{-1}$ s^{-1}. The present k_1(298 K) results are in reasonable agreement with two previous 296 K (760 Torr, syn. air) relative rate measurements. The rate coefficient for the Cl-atom + PCBTF reaction, k_2, was also measured in THALAMOS using a relative rate technique that yielded $k_2(298\ K) = (7.8 \pm 2) \times 10^{-16}$ cm^3 $molecule^{-1}$ s^{-1}. As part of this work, the UV and infrared absorption spectra of PCBTF were measured (NOAA; Boulder, CO, USA). On the basis of the UV absorption spectrum, the atmospheric instantaneous UV photolysis lifetime of PCBTF (ground level, mid-latitude, Summer) was estimated to be 3–4 days, assuming a unit photolysis quantum yield. The non-Arrhenius behavior of the OH + PCBTF reaction over the temperature range 275 to 950 K is interpreted using a mechanism for the formation of an OH-PCBTF adduct and its thermochemical stability. The results from this study are included in a discussion of the OH radical and Cl atom kinetics of halogen substituted aromatic compounds for which only limited temperature dependent kinetic data are available.

Introduction

The gas-phase OH radical kinetics of substituted aromatic compounds has been the subject of research for decades, e.g. Calvert et al.,[1] Thiault et al.,[2] Thüner et al.,[3] and Seta et al.[4] and references cited within. However, there remains limited insight into the reaction mechanisms and the formation of pre-reactive complexes, OH-aromatic adduct formation and thermal stability, as well as degradation products. More recently, theoretical methods have been used to interpret the reaction potential energy surface (PES) of these reactions,[5-7] but the ability to validate the calculations by comparison with experimental data is rather limited.

4-chlorobenzotrifluoride ($C_7H_4ClF_3$, para-chlorobenzotrifluoride, PCBTF) (see **Figure 1**) is a volatile chemical product (VCP) used in solvent-based coatings, e.g. paint, that is released into the atmosphere during application. VCPs have been identified as possible contributors to ozone and secondary organic aerosol (SOA) formation, and thus, impact air quality in urban environments.[8,9] Gkatzelis et al.[9] recently observed PCBTF in urban environments and identified it as a major component of solvent-based coating emissions.

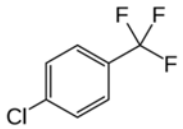

Figure 1. 4-chlorobenzotrifluoride (p-$ClC_6H_4CF_3$, para-chlorobenzotrifluoride, PCBTF)

Atkinson et al.[10] and Young et al.[11] used relative rate methods and reported 296 K rate coefficients for the OH reaction:

$$OH + PCBTF \rightarrow \text{products} \quad (1)$$

of $(2.3 \pm 0.8) \times 10^{-13}$ and $(2.22 \pm 0.30) \times 10^{-13}$ cm^3 $molecule^{-1}$ s^{-1}, respectively. Young et al. also identified 2-chloro-5-trifluoromethylphenol (o-CTFP) as a primary reaction product, which implies a reaction mechanism involving the formation of an OH-PCBTF adduct.

In this work, absolute rate coefficients for the OH + PCBTF reaction were measured over a broad range of temperature (275 to 950 K) using low-pressure discharge flow tube reactors coupled to a mass spectrometer detector (ICARE/CNRS, Orleans, France) and over the temperature range 298–353 K using a relative rate method in the thermally regulated atmospheric simulation chamber THALAMOS (Douai, France). Rate coefficients for the Cl-atom reaction:

$$Cl + PCBTF \rightarrow \text{products} \quad (2)$$

were measured using a relative rate method at 298 K (760 Torr, syn. air) in THALAMOS. In addition, theoretical methods have been applied to investigate the reaction mechanisms of reactions 1 and 2. The theoretical methods were applied to describe the OH- and Cl-PCBTF adduct thermochemical stability as well as a general interpretation of the observed non-Arrhenius behavior of k_1(T). A comparison of the present OH radical and Cl-atom reaction rate coefficients with literature values for other aromatic compounds and insights into the reactivity trends are discussed. This work provides insight into the reactivity and reaction mechanisms of substituted aromatic compounds of interest to atmospheric and combustion chemistry. Infrared and UV spectra for PCBTF are reported in this work. To the best of our knowledge, the present study is the first to report a PCBTF infrared absorption spectrum, which enables estimates of climate metrics, e.g., radiative efficiency (RE) and global warming potential (GWP). The presently reported PCBTF UV spectrum extends into the tropospheric actinic region, wavelengths greater than 295 nm, thus enabling atmospheric photolysis rate calculations.

Experimental Details

This work includes experimental laboratory measurements made using: (1) a low-pressure discharge flow-tube with mass spectrometer detection, (2) the THALAMOS environmental chamber for kinetic studies of reactions 1 and 2, and (3) UV and infrared absorption spectra setups. The UV and infrared absorption spectra of PCBTF were measured as part of this work (NOAA, Boulder, CO, USA). The UV spectrum measurements extended into the tropospheric actinic region, wavelengths (λ) greater than 295 nm, which enable more reliable estimates of the PCBTF atmospheric photolysis lifetime. The experimental apparatus and methodologies are described separately below.

Low-pressure discharge flow-tube reactor (ICARE/CNRS). Kinetic measurements for the OH + PCBTF reaction were performed over the temperature range 275–950 K using a flow tube reactor coupled with a modulated molecular beam sampling electron-impact ionization mass spectrometer (MS).[12-15] As described in detail elsewhere,[15] low- and high-temperature flow-tube reactors were used in this study. The low-temperature reactor (275–340 K), see **Figure S1**, was a jacketed Pyrex tube (45 cm length and 2.4 cm i.d.) with its temperature regulated by circulating a thermostated fluid through the jacket. The flow-tube reactor and movable injector were coated with halocarbon wax. The high-temperature reactor (385–950 K), see **Figure S2**, was made of quartz (45 cm length and 2.5 cm i.d.) and its temperature was controlled by an electrical heater.[14,15]

Measurements of k_1(T) were performed using absolute and competitive reaction methods. Absolute k_1(T) measurements were made at a total pressure of 4.0–4.2 Torr (He) under pseudo first–order conditions in the OH radical, i.e., [OH] <<[PCBTF], where the loss of OH is given by:

$$[OH]_t = [OH]_0 \times \exp(-k_1't) \quad (I)$$

and $k_1' = k_1 \times [PCBTF] + k_w$. k_w is the first-order rate coefficient for the heterogeneous wall-loss of the OH radical. Typical values of k_w were 5–15 s^{-1}. Pseudo first–order rate coefficients, k_1', were corrected for axial and radial diffusion of OH radicals[16] with a diffusion coefficient of OH in He of $D_0 = 660 \times (T/298)^{1.85}$ Torr cm^2 s^{-1}.[17] The corrections were typically <6%.

Hydroxyl radicals were produced in the movable injector by the reaction of the H-atom with NO_2 that was present in excess:

$$H + NO_2 \rightarrow OH + NO \quad (3)$$

where k_3(195–2000) = (1.47 ± 0.26) × 10^{-10} cm^3 $molecule^{-1}$ s^{-1}.[18] H-atoms were generated in a H_2/He microwave discharge mounted on the movable injector.

OH radicals were titrated by the addition of Br_2 (5 × 10^{13} molecule cm^{-3}) at the end of the flow-tube reactor, ~5 cm upstream of the MS sampling cone:

$$OH + Br_2 \rightarrow HOBr + Br \quad (4)$$

where k_4(220–950 K) = 2.16 × 10^{-11} exp(207/T) cm^3 $molecule^{-1}$ s^{-1}.[12] HOBr was monitored by MS at m/z = 98 ($HOBr^+$) as an indirect measurement of the OH radical. The absolute OH radical concentration was determined using the stoichiometry of reaction 4, [OH] = [HOBr] = Δ[Br_2], with the measured Δ[Br_2] calibrated using the Br_2 parent MS peak and calibrated standard samples. The initial OH radical concentration, $[OH]_0$, over the course of this study was in the (0.8–2.5) × 10^{11} molecule cm^{-3} range. A detailed discussion of the possible influence of secondary chemistry in this monitoring/calibration method has been presented previously.[19,20] The PCBTF concentration was varied over the course of the experiments in the range (0.1–14.6) × 10^{14} molecule cm^{-3}.

The second flow-tube kinetic method used in this study applied a competitive reaction approach. Measurements of k_1(T) were conducted in competition with the reaction of OH with Br_2. Experiments were performed over the 295 to 770 K temperature range at total pressures in the 2.0–8.2 Torr (He) range. k_1(T) was determined by the measurement of the HOBr yield as a function of the [PCBTF]/[Br_2] ratio in the flow-tube. The fraction of $[OH]_0$ transformed to HOBr in reaction 4 is given by:

$$[HOBr] = \frac{k_4[Br_2]}{k_4[Br_2]+k_1[PCBTF]+k_w} \times [OH]_0 \quad (II)$$

Rearrangement of eq. II yields:

$$\frac{[OH]_0}{[HOBr]} - 1 = \frac{k_1[PCBTF]}{k_4[Br_2]} + \frac{k_W}{k_4[Br_2]} \quad \text{(III)}$$

For a constant Br_2 concentration, the far right-hand term in eq. III is constant and k_1/k_4 is determined from ($[OH]_0/[HOBr]$ - 1) vs $[PCBTF]/[Br_2]$. In the experiments, HOBr was monitored with and without PCBTF added to the system. In these experiments, the reaction time was (0.05–0.06) s and $[OH]_0$, [PCBTF], and $[Br_2]$ were in the ranges (1–4) × 10^{11} molecule cm^{-3}, (0.32–11.8) × 10^{14} molecule cm^{-3}, and (3–5) × 10^{13} molecule cm^{-3}, respectively.

The PCBTF concentration and MS calibration (m/z = 180, $PCBTF^+$) was determined from measured gas flows and pressure. In addition, a 0.6–1.0 μL of PCBTF was injected into the He carrier gas flow and the PCBTF signal recorded. The PCBTF calibration determined by these two methods agreed to within 10%.

THALAMOS (Douai, France). THALAMOS is a temperature regulated 0.6 m^3 Teflon atmospheric chemistry simulation chamber. Details of the chamber and measurement capabilities are provided elsewhere.[21,22] Fourier transform infrared spectroscopy (FTIR) with an optical path of 10 m and Selected Ion Flow Tube Mass Spectrometry, SIFT-MS, were used in the present study to monitor the loss of reactants within the chamber.

k_1(298–353 K) and k_2(298 K) were measured at 760 Torr (syn. air) using a relative rate method.

$$k = k_{Ref} \times \ln([PCBTF]_t/[PCBTF]_0 / \ln([Ref]_t/[Ref]_0) \quad \text{(IV)}$$

C_2H_6, CH_2Cl_2, and CH_3CCl_3 were used as reference compounds:[23]

$$OH + C_2H_6 \qquad k(T) = 7.66 \times 10^{-12} \exp(-1020/T) \text{ cm}^3 \text{ molecule}^{-1} \text{ s}^{-1} \quad (5)$$

$$OH + CH_2Cl_2 \qquad k(T) = 1.92 \times 10^{-12} \exp(-880/T) \text{ cm}^3 \text{ molecule}^{-1} \text{ s}^{-1} \quad (6)$$

and

$$Cl + CH_3CCl_3 \qquad k(T) = k(298 \text{ K}) = 9.0 \times 10^{-15} \text{ cm}^3 \text{ molecule}^{-1} \text{ s}^{-1} \quad (7)$$

OH radicals were produced by the broadband photolysis (10 UV-A lamps) of HONO:

$$HONO + h\nu \rightarrow OH + NO \quad (8)$$

The reaction chamber total pressure was maintained at 760 Torr with the flow out of the chamber balanced with an input bath gas flow. The reaction chamber dilution was measured using the observed loss of CCl_4, which was added to the reaction mixture at the start of the experiment. The first-order chamber dilution was in the range (1.0–1.2) × 10^{-5} s^{-1} over the course of the

experiments. The first-order loss of PCBTF in the absence of OH radical production, k_d, was measured prior to each kinetic measurement:

$$\text{PCBTF} \rightarrow \text{loss} \quad (9)$$

The dark loss of PCBTF was in the range (1.6–1.8) × 10^{-5} s^{-1}, i.e., dilution and dark loss combined. The duration of a kinetic measurement was typically ~1 hour and the dark loss of PCBTF in most cases accounted for 2–3% (maximum of 10%) of the observed PCBTF loss. The reference compound loss, k'_d, was entirely due to flow out of the system, i.e., no wall loss. The relative rate expression is therefore given as:

$$\frac{1}{(t-t_0)}\ln\frac{[PCBTF]_{t_0}}{[PCBTF]_t} - k_d = \frac{k_1}{k_{ref}}\left[\frac{1}{(t-t_0)}\ln\frac{[Ref]_{t_0}}{[Ref]_t} - k'_d\right] \quad (V)$$

where t_0 is the start of the kinetic measurements.

k_2(298 K) was measured under static conditions using SIFT-MS detection[24] to monitor the loss of PCBTF and the reference compound CH_3CCl_3. PCBTF loss was determined by continuous monitoring of its characteristic mass peaks upon reaction with H_3O^+ (m/z 161, $ClC_6H_4CF_2^+$), NO^+ (m/z 210, $ClC_6H_4CF_3$-NO^+) and O_2^+(m/z 180, $ClC_6H_4CF_3^+$). CH_3CCl_3 loss was monitored using the $CH_3CCl_2^+$ ion, m/z: 97 and the O_2^+ reagent ion. Cl atoms were produced in the UV-A photolysis of Cl_2:

$$Cl_2 + h\nu \rightarrow 2\ Cl \quad (9)$$

Experiments lasted approximately 2 hours. The SIFT-MS sampling flow out of the system, ~10 sccm, had a negligible impact on the pressure and concentrations in the reactor over the duration of an experiment. The PCBTF first-order dark loss was measured to be ~5 × 10^{-6} s^{-1}. The PCBTF dark loss accounted for a ~20% correction to the observed PCBTF loss. The dark loss correction contributed ~10% uncertainty in the determination of k_2(298 K). CH_3CCl_3 dark loss was measured to be negligible.

UV Absorption Spectrum Measurements. The gas-phase UV absorption spectrum, $\sigma(\lambda)$, of PCBTF was determined by applying Beer's law:

$$A(\lambda) = \sigma(\lambda) \times L \times [\text{PCBTF}] \quad (VI)$$

where $A(\lambda)$ is the measured absorbance at wavelength λ, $\sigma(\lambda)$ is the absorption cross section of PCBTF, and L is the absorption pathlength. Absorption cross sections were determined in separate measurements over the wavelength range 200–360 nm using a 0.5 m spectrometer with a 512 × 2048 charge couple device (CCD) detector and at 213.9 nm using Zn lamp source. Broadband

spectra were measured using a 30 W D_2 lamp with a 90.4 cm single pass absorption cell. Atomic line absorption measurements were made using Pen-ray Zn lamp light source, a 25.5 cm single pass Pyrex absorption cell with quartz windows, and photodiode detectors with 214 nm bandpass filters. All measurements were performed at 296 K.

The PCBTF concentration was quantified using absolute pressure measurements of dilute PCBTF mixtures prepared manometrically off-line. To improve and extend the CCD spectrum determination into the long-wavelength region, the PCBTF concentration was optimized for the <220 nm and >230 nm regions in separate measurements. The spectra were combined using the overlapping region to obtain the final spectrum. The accuracy of the UV absorbance measurement was ~5% between 200 and 280 nm and ~10% between 280 and 320 nm. The absolute uncertainty in σ(213.9 nm) is estimated to be ~5%.

Infrared Absorption Spectrum Measurements. Infrared absorption spectra of PCBTF were measured at 296 K using Fourier transform infrared (FTIR) spectroscopy between 500 and 4000 cm^{-1} at 0.5 cm^{-1} resolution. The FTIR was coupled to a multi-pass absorption cell (KBr windows) with a 485 cm optical pathlength. The detector was a liquid nitrogen cooled HgCdTe (MCT) semi-conductor. The PCBTF infrared absorption spectrum was quantified using absolute pressure measurements. The PCBTF concentration was determined using the measured absolute pressure, the mixing ratio of the dilute sample, and the ideal gas law. At least 8 different pressures of the dilute mixtures (PCBTF/N_2), between 8.0 and 100.7 Torr, were used for each set of measurements. The range of concentration used in the absorption measurements was (5.4–36) × 10^{15} molecule cm^{-3}.

Materials. In the Douai and CNRS studies, the PCBTF sample was of 98% purity. The Cl_2 purity was 99.8%. The purities of the gases used in the CNRS discharge flow experiments were: He (>99.9995%), passed through liquid nitrogen trap; H_2 (>99.998%); Br_2 (>99.99%); NO_2 (>99%). In the flow-tube experiments, PCBTF was delivered to the flow-tube by passing bath gas (He) over a liquid PCBTF sample. In the Douai studies, HONO was synthesized, in situ, by adding 0.1 M aqueous $NaNO_2$ dropwise (~0.5 ml min^{-1}) into ~50 ml of 0.5 M (10% v/v) or 1 M (20% v/v) aqueous solution of H_2SO_4. A continuous flow of N_2 (~500 sccm) over the headspace of solution was used to sweep HONO into the chamber. NO_2 was monitored in several measurements via FTIR to establish that the NO_2 concentration was sufficiently low enough to not interfere with the relative rate (RR) kinetic measurements. In the NOAA studies, para-chlorobenzotrifluoride (*p*-

$ClC_6H_4CF_3$, PCBTF, CAS RN: 98-56-6) was obtained commercially with a stated purity of >99%. The PCBTF sample was stored in a glass vacuum reservoir and degassed prior to use. Dilute mixtures of PCBTF in a N_2 (UHP, 99.999%)-bath gas, 0.092 and 0.0595% with a total pressure of ~800 Torr, were manometrically prepared in a 12 L Pyrex bulb with a mixing ratio uncertainty of ~2%. The bulb mixtures were stable over the duration of the study as confirmed by infrared absorption measurements. Pressures were measured using calibrated 10, 100, and 1000 Torr capacitance manometers. Uncertainties given throughout the paper are 2σ unless noted otherwise.

Computational Methods

The thermochemistry of the reaction channels for the OH radical and Cl atom + PCBTF reactions were investigated theoretically. All OH- and Cl-adduct formation channels and the subsequent H_2O and HCl elimination products were investigated using quantum mechanical molecular calculations. PCBTF, H_2O, HCl, pre-reactive complexes, all possible OH- and Cl-adducts, and dehydrogenated radical geometries were fully optimized at all equilibrium points using the M06-HF[25,26] method in conjunction with the TZVP[27,28] basis set. In the case of OH-pre-reactive complexes geometry optimization, a variety of different initial geometries were tested, trying to direct both the hydrogen and the oxygen atom of the OH radical towards the aromatic ring. Single-point energy calculations were further performed at the CCSD(full)/TZVP//M06-HF/TZVP[29-32] level of theory to improve the electronic energy accuracy of the optimized lowest energy structures. In accordance with the reliability of the CCSD(full) calculations and the previously well-known M06-HF, balanced mean unsigned errors for thermochemistry, kinetics, and non-covalent interactions[33-35] error expectations should remain less than 5 kJ mol^{-1} for the aforementioned reactions. Global minimum structures were validated by vibrational analysis at the M06-HF/TZVP level of theory and verified by the lack of any negative frequency values. Both M06-HF and CCSD calculations were carried out by using the GAUSSIAN09 [36] suite of programs.

Results and Discussion

Results from the low-pressure discharge flow-tube and THALAMOS kinetic studies and the UV and infrared absorption measurements are presented separately below.

Flow-tube absolute measurements of k_1. A summary of the experimental conditions and k_1(T) values obtained is given in **Table 1** and displayed in **Figure 2**. **Figure S3** displays a

representative set of pseudo first-order kinetic data obtained at 645 K for OH loss in the presence of a range of PCBTF concentrations. OH loss was observed to be exponential with a eq. I fit precision of ~3%. Experimental data obtained at other temperatures are of similar quality and precision. A second-order plot of representative high-temperature kinetic data is shown in **Figure 3. Figure S4** shows representative data obtained between 275 and 340 K. The data show a linear dependence on the PCBTF concentration with a 2–5% fit precision, see **Table 1**.

Table 1. Summary of the experimental conditions and rate coefficients, k_1(T), for the OH + *p*-$ClC_6H_4CF_3$ (PCBTF, para-chlorobenzotrifluoride) reaction obtained using the absolute discharge flow-tube method

Temperature (K) [a]	[PCBTF] Range (10^{14} molecule cm^{-3})	Number of PCBTF Concentrations	k_1 [b] (10^{-13} cm^3 molecule^{-1} s^{-1})
275	0.44–4.77	9	1.99 ± 0.06
290	0.24–5.85	9	1.61 ± 0.03
298	0.17–5.90	9	1.63 ± 0.03
303	0.15–5.04	10	1.53 ± 0.02
317	0.15–5.70	8	1.39 ± 0.03
325	0.19–6.42	10	1.30 ± 0.03
340	0.15–6.01	10	1.16 ± 0.02
370	0.89–9.29	9	1.01 ± 0.02
385	0.19–11.9	10	0.94 ± 0.01
400	0.52–14.6	8	0.67 ± 0.01
410	0.21–12.3	9	0.54 ± 0.01
420	0.21–12.4	10	0.35 ± 0.01
470	0.69–12.5	9	0.26 ± 0.01
490	0.30–10.4	10	0.31 ± 0.06
500	0.41–11.2	10	0.36 ± 0.01
540	0.98–9.92	7	0.54 ± 0.02
585	0.19–6.60	8	0.79 ± 0.02
645	0.32–9.09	8	1.07 ± 0.02
720	0.25–6.07	9	1.62 ± 0.04
820	0.12–4.19	8	2.65 ± 0.04
950	0.10–4.75	10	3.63 ± 0.06

[a] Halocarbon wax coated reactor at 275–340 K and uncoated quartz reactor at 370–950 K;
[b] Quoted error limits are 2σ of the measurement precision, the total estimated uncertainty in k_1 is ~15% (2σ) at all temperatures

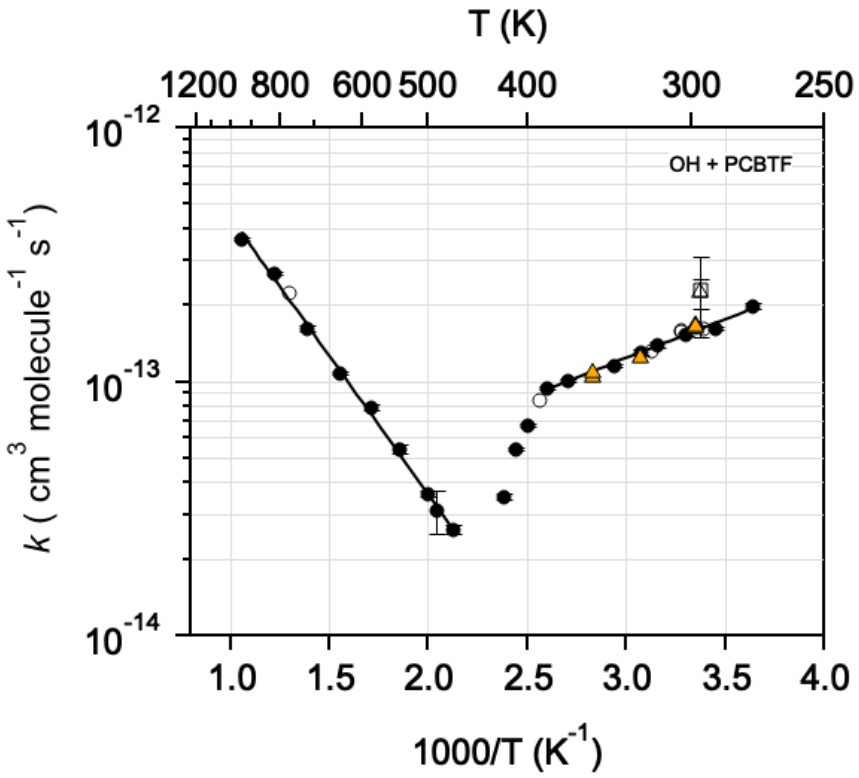

Figure 2. Summary of OH + PCBTF rate coefficient, k_1(T), measurements. This work, discharge flow-tube studies: absolute (solid circles, see **Table 1**); competitive reaction method (open circles, see **Table 2**). Solid lines are least-squares fits (see text), THALAMOS relative rate measurements are given as solid triangles. Literature data: Atkinson et al.[10] (open square); Young et al.[11] (open triangle).

k_1(T) displays a complex temperature dependence over the broad temperature range of our measurements. In the low-temperature regime, k_1(T) displays a negative temperature dependence with the temperature dependence at ≤385 K represented by the Arrhenius expression:

$$k_1(275–385\ \text{K}) = (1.50 \pm 0.15) \times 10^{-14} \exp((705 \pm 30)/\text{T})\ \text{cm}^3\ \text{molecule}^{-1}\ \text{s}^{-1}$$

At temperatures between 400 and 420 K, a strong decrease in k_1(T) is observed that is attributed to the decomposition of the weakly bound association reaction adduct (see the OH and Cl Reaction Mechanisms section). At temperatures ≥470 K, k_1(T) displays a strong positive Arrhenius temperature dependence given by:

$$k_1(470–950\ \text{K}) = (5.42 \pm 0.40) \times 10^{-12} \exp(-(2507 \pm 45)/\text{T})\ \text{cm}^3\ \text{molecule}^{-1}\ \text{s}^{-1}$$

The uncertainties given in above equations for k_1 are from the fit precision.

It should be noted that at the lower-end of the temperature ranges for both reactors that k_w (OH wall loss) increased, see **Figure S4**. This indicates a possible contamination of the reactor surface

by PCBTF and/or products of reaction 1. The increase in k_w significantly impacted measurements at temperatures <275 K in the halocarbon coated flow-tube and <370 K in the uncoated quartz flow-tube. This established the low-temperature limits in these measurements.

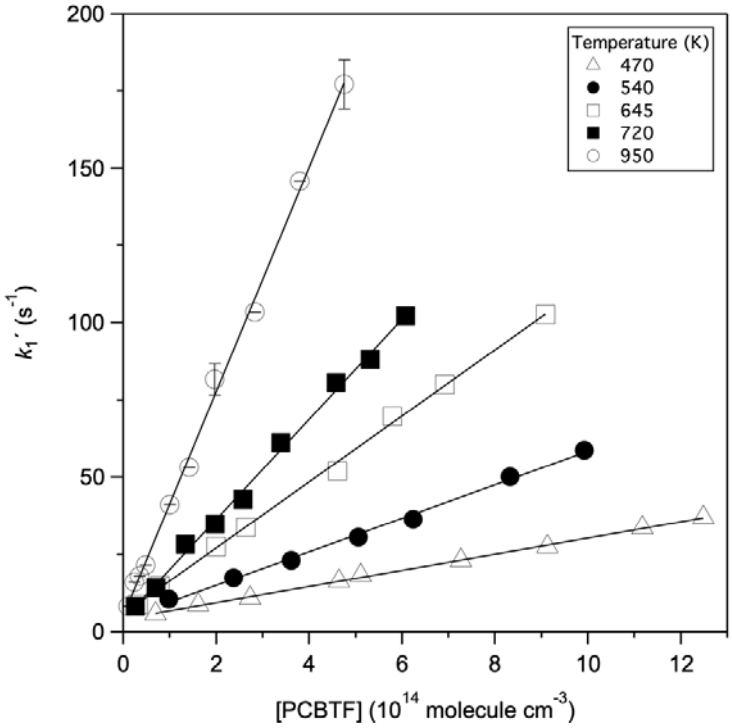

Figure 3. Representative pseudo first-order rate coefficient, k_1', data for the OH + PCBTF reaction measured using the absolute discharge flow-tube method. For improved clarity, only a few representative data error bars are shown. Typical uncertainties are ≤5%.

The possible impact of secondary chemistry on our k_1 flow tube measurements was tested in measurements performed using different $[OH]_0$ values, see **Figure S4**. Results obtained with $[OH]_0$ varied by a factor of 2.5 were indistinguishable to within the experimental precision, ~3%, which implies secondary chemistry was not important. The potential impact of sample impurities on the measurements of k_1 was evaluated by comparing results obtained using the original PCBTF sample and purified samples. PCBTF samples were purified by vacuum distillation and using several freeze–pump–thaw cycles. The kinetic data obtained with the purified and original samples were similar. An overall decrease in the volume of the PCBTF liquid sample by an order of magnitude, over the course of the experiments, also did not impact the results. These tests suggest that impurities had a negligible impact on the k_1 determination. This is also supported by comparison of our data with the results of our relative rate measurements presented below. The combined

uncertainty in the absolute flow-tube measurements of k_1(T) is estimated to be ~15% by adding in quadrature statistical error (<4%) and uncertainties in the PCBTF concentration (~10%), gas flows (3%), pressure (2%), and temperature (~1%).

Flow-tube competitive reaction (CR) measurements of k_1(T). A summary of the experimental conditions and k_1(T) values obtained in the flow-tube CR experiments is given in **Table 2**. Examples of typical experimental CR data are shown in **Figure 4**. The rate coefficient for the OH + Br_2 reference reaction, k_4(T), with an estimated 10% absolute uncertainty over the 220–950 K temperature range, was taken from a previous study from the ICARE, CNRS laboratory.[12] The values of k_1(T) obtained with the CR method are included in **Figure 2** and agree with the absolute flow-tube measurement results at all temperatures, to within ~2%.

Table 2. Summary of the experimental conditions and obtained rate coefficients, k_1(T), for the OH + PCBTF reaction using the flow-tube competitive reaction (CR) method

Temperature (K)	[PCBTF] Range (10^{14} molecule cm^{-3})	Number of [PCBTF] data points	[Br_2 (10^{12} molecule cm^{-3})	k_1/k_4 × 1000 [a]	k_1(T) (10^{-13} cm^3 molecule^{-1} s^{-1}) [c]
295 [d]	0.65–6.81	10	3.75	3.72 ± 0.11	1.62 ± 0.24
305 [d]	0.61–8.88	10	5.80	3.75 ± 0.06	1.60 ± 0.24
305 [e]	0.44–11.8	9	3.70	3.70 ± 0.05	1.58 ± 0.24
320 [d]	0.75–8.41	9	4.01	3.21 ± 0.06	1.32 ± 0.20
390 [f]	0.54–15.5	8	4.06	2.30 ± 0.04	0.85 ± 0.13
770 [f]	0.32–11.2	11	3.15	7.86 ± 0.09	2.23 ± 0.33

[a] 2σ of the measurement precision; [b] $k_4(T) = 2.16 \times 10^{-11} \exp(207/T)$ cm^{3}molecule^{-1}s^{-1}; [c] the total estimated uncertainty in k_1 is ~15% (2σ) at all temperatures [d] Halocarbon wax coated reactor, 2 Torr; [e] Halocarbon wax coated reactor, 8.2 Torr; [f] Uncoated quartz reactor, 4 Torr.

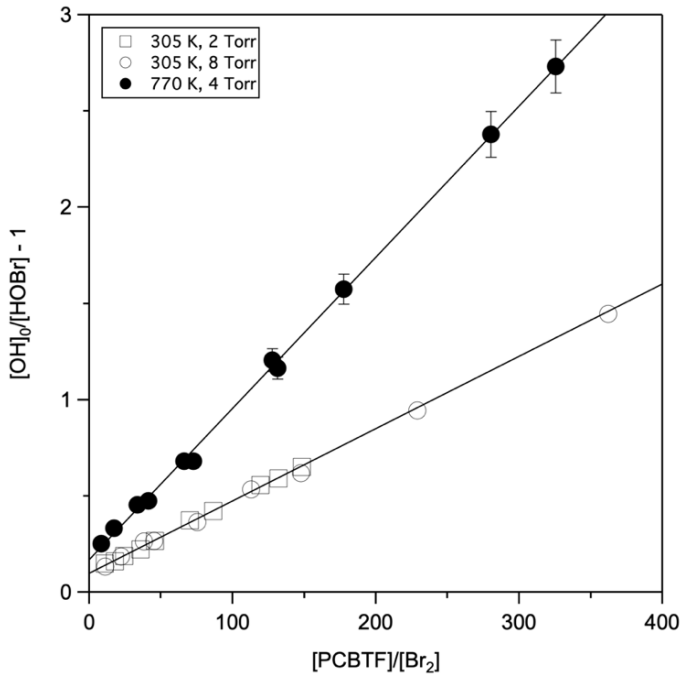

Figure 4. Yield of HOBr from OH-radical titration by Br_2 + PCBTF mixtures at 305 and 770 K. Partially visible error bars represent measurement precision uncertainties, ~5%. The 305 K data at 8.2 Torr are shifted to provide an intercept similar to that obtained in the 2 Torr experiment.

THALAMOS k_1(T) RR measurement. Experimental conditions and results obtained from the relative rate measurements of reaction 1 at 298, 325, and 353 K are summarized in **Table 3**. The experimental data obtained at 298 K are shown in **Figure 5**. Typical experiments at different temperatures are shown in **Figures S5** and **S6**. The two independent 298 K experiments performed with the C_2H_6 reference and the single measurement with the CH_2Cl_2 reference compound were in good agreement with k_1(298 K) values of $(1.65 \pm 0.1) \times 10^{-13}$ cm^3 molecule^{-1} s^{-1} and $(1.62 \pm 0.07) \times 10^{-13}$ cm^3 molecule^{-1} s^{-1}, respectively. The RR results obtained at 298, 325, and 353 K are in excellent agreement with the discharge flow-tube results from this study (see **Figure 2**).

Table 3. Summary of experimental conditions and obtained rate coefficient results for the gas-phase OH + p-$ClC_6H_4CF_3$ (para-chlorobenzotrifluoride, PCBTF) reaction obtained in this work, using a relative rate method

T (K)	$[PCBTF]_o$ (10^{14} molecule cm^{-3})	$[CH_2Cl_2]_o$ (10^{14} molecule cm^{-3})	$[C_2H_6]_o$ (10^{14} molecule cm^{-3})	k_{PCBTF}/k_{Ref} [a]	k_{PCBTF} [b] (10^{-13} cm^3 molecule^{-1} s^{-1})
298	12.4	12.6	–	1.62 ± 0.07	1.62 ± 0.25
298	4.96	–	4.96	0.67 ± 0.02	1.66 ± 0.10
298	4.96	–	7.43	0.66 ± 0.01	1.64 ± 0.09
325	4.96	10.4	–	0.97 ± 0.03	1.24 ± 0.23
353	4.96	10.4	–	0.67 ± 0.01	1.06 ± 0.24
353	4.96	10.4	–	0.67 ± 0.02	1.07 ± 0.26

[a] 2σ fit precision; [b] 2σ uncertainty including estimated systematic uncertainties, rate coefficients were derived using for OH + C_2H_6, k(298 K) = $(2.5 \pm 0.12) \times 10^{-13}$, k(T) = 7.66×10^{-12} exp(-1020/T)

and for OH +CH_2Cl_2, k(T) = 1.92 × 10^{-12} exp(-880/T), k(298 K) = (1.0 ± 0.15)×10^{-13}, in cm^3 $molecule^{-1}$ s^{-1}.[23]

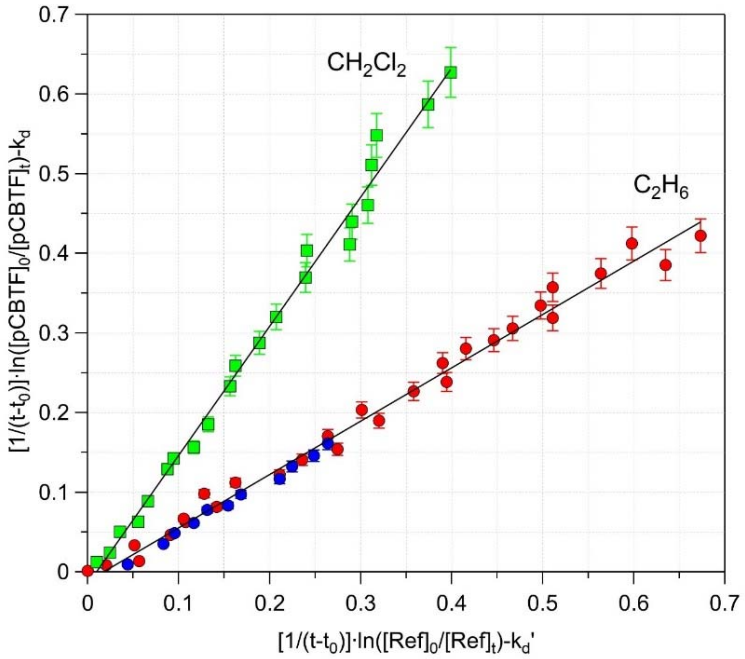

Figure 5. Relative rate data obtained in the determination of the OH + PCBTF rate coefficient at 298 K and 760 Torr. Circles and squares represent measurements performed using OH + C_2H_6 and CH_2Cl_2 as reference reactions, respectively. The different color symbols for C_2H_6 denote independent experiments. Results are summarized in **Table 3**.

As part of this study, pulsed laser photolysis-laser induced fluorescence (PLP-LIF) absolute kinetic measurements of reaction 1 were performed at 298 K. The measurements, however, yielded unreliable OH radical production and decay profiles in the presence of PCBTF over time. We attribute these problems to cumulative contamination of the LIF reactor following kinetic measurements. Therefore, we have chosen not to report the detailed results from the PLP-LIF experiments. Note, however, that in what we consider our best kinetic measurement, i.e., in a clean LIF reactor, the obtained k_1(298 K) agreed with the results from the flow-tube and relative rate experiments to within 5%.

Comparison with previous k_1(298 K) studies. Atkinson et al.[10] and Young et al.[11] have reported k_1(296 K) obtained in relative rate studies prior to this study with values of (2.3 ± 0.80) × 10^{-13} cm^3 $molecule^{-1}$ $s^{-1}$and (2.22 ± 0.30) × 10^{-13} cm^3 $molecule^{-1}$ s^{-1}, respectively. Both studies obtained k_1(296 K) values slightly greater than obtained in the present study by ~30%. Their results are included in **Figure 2** for comparison with the present work.

It is possible that the discrepancy is due to PCBTF loss other than reaction with the OH radical in the literature RR studies. This would lead to an overestimate of k_1(296 K). However, we have no evidence from the published literature available that would confirm this hypothesis.

The present measurements of k_1(T) were performed over a range of pressures from 2 Torr (He) to 760 Torr (syn. air). k_1(298 K) values obtained over this pressure range agreed to within 5%, which indicates that reaction 1 is near its high-pressure limit over this pressure range at 298 K. Note that in the 390 to 470 K temperature range the reaction is most likely in the fall-off region for our low-pressure measurements.

The k_1(298 K) measured in this work is compared with rate coefficient data for other aromatic compounds in **Table 4**. It is apparent that the combined para- Cl- and CF_3-substitution to the benzene ring reduces the OH reactivity of the aromatic compound by one order of magnitude. This decrease in reactivity with halogen substitution is also demonstrated for the chlorobenzene and *p*-dichlorobenzene reactions, with the decrease being more pronounced with increasing halogen addition to the ring. As in the PCBTF reaction, replacing the Cl- substitution by a CF_3- group decreases the OH reactivity by an additional factor of ~3. This implies that stereochemical and electronic withdrawing effects of the CF_3-group substitution reduces the probability of OH radicals forming a pre-reactive complex, i.e., OH reactivity is strongly dependent on the group-type attached in the aromatic ring. This is illustrated further in the case of phenol where its reactivity is ten times greater than for benzene and more than two orders of magnitudes greater compared to PCBTF. OH reactivity is further increased in the case of aniline, most likely due to the activation of H-abstraction channels (-NH_2) that react without distorting the ring-aromaticity. Greater OH reactivity is also observed for other substituted aromatic compounds with H-donor groups attached to the ring, such as toluene (-CH_3), xylene (2 ×-CH_3), trimethyl-benzene (3 ×-CH_3), cresol (-OH and CH_3), methoxy-benzene (-O-CH_3), ethyl-toluene (-CH_3 and CH_2CH_3), ethyl-benzene (-CH_2CH_3), and propyl-benzene (-$CH_2CH_2CH_3$). It is also worthwhile to note that in all cases, compounds with two groups attached on the ring as *m*-isomers are substantially more reactive, while *o*- and *p*-isomers exhibit similar reactivity. Finally, comparing the effect of -CF_3 (benzotrifluoride) and -Cl (chloro-benzene) groups on aromatic compound reactivity towards the OH radical, the -CF_3 substitution leads to a smaller OH rate coefficient by a factor of two.

Table 4. Comparison of OH reactivity, k(298 K), for monocyclic aromatic compounds

Aromatic	Structure	$k^{a,b}$	Aromatic	Structure	$k^{a,b}$
Benzene	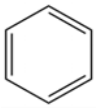	1.2	Aniline	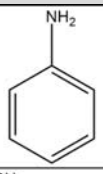	120
Toluene	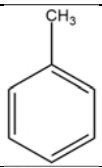	5.9	*o*-Ethyltoluene	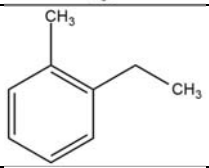	13.0
o-Xylene	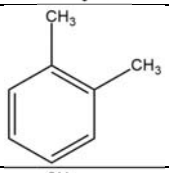	14.3	*m*-Ethyltoluene	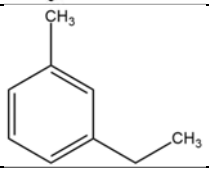	18.0
m-Xylene	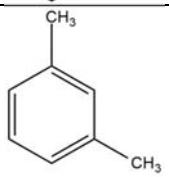	24.0	*p*-Ethyltoluene	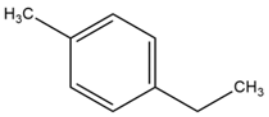	12.0
p-Xylene	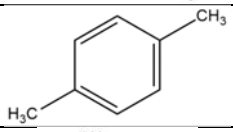	15.3	Ethylbenzene	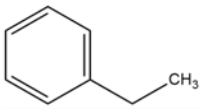	7.8
1,2,3-trimethylbenzene	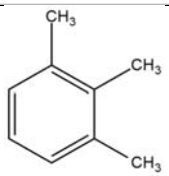	33.3	*n*-Propylbenzene	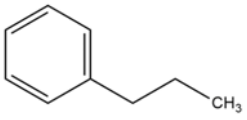	5.8
1,2,4-trimethylbenzene	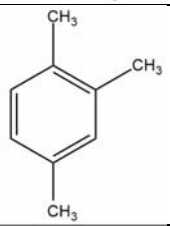	40.0	Chlorobenzene	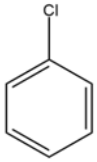	0.88
1,2,5-trimethylbenzene	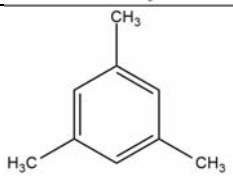	62.4	*o*-Dichlorobenzene	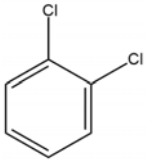	0.42
Phenol	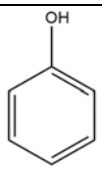	28.0	*m*-Dichlorobenzene	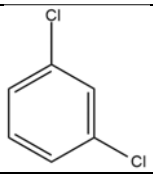	0.72

o-Cresol	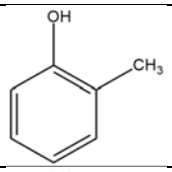	38.0	*p*-Dichlorobenzene	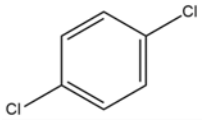	0.32
m- Cresol	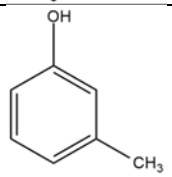	56.0	1,2,4-Trichlorobenzene	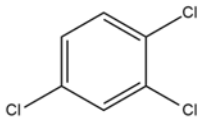	0.50
p- Cresol	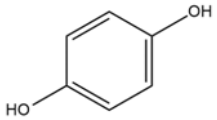	42.0	Benzotrifluoride	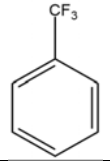	0.44
Methoxybenzene	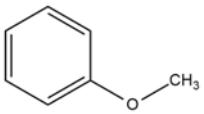	16.0	PCBTF	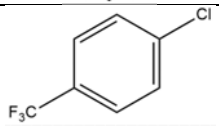	0.16

[a] units of rate coefficient at 298 K, k(298 K), in units of 10^{-12} cm^3 molecule^{-1} s^{-1}; [b] Rate coefficients were taken from NIST Kinetic Database[37]and references within.

THALAMOS k_2(298 K) RR measurement. The experimental conditions and results obtained in the Cl + PCBTF reaction relative rate measurements are summarized in **Table 5**. **Figure 6** shows a representative set of relative rate data from one of the experiments. Data from the other two experiments are shown in **Figures S7 and S8**. Note that although the Cl + CH_3CCl_3 reference reaction is ~12 times greater compared to Cl +PCBTF, it was selected mainly because its rate coefficient is reasonably well-established, which is uncommon for reactions with rate coefficients on the order of 10^{-16} cm^3 molecule^{-1} s^{-1}. The PCBTF-O_2^+ data showed the highest precision, although the fit precision of the experimental data was better than 7% (1σ) in all cases (see **Table 5**). An average of the different ion rate coefficient ratios, k_{PCBTF}/k_{Ref}, was used in the final analysis. The results from the three independent experiments agree to within 3%, with an average k_2(298 K) value of (7.8 ± 2) × 10^{-16} cm^3 molecule^{-1} s^{-1}, where the quoted uncertainty includes estimated systematic errors and the reference reaction estimated uncertainty. Since our measurements have been conducted in the presence of O_2, secondary OH formation, similarly to other aromatic compounds,[38] might lead to an overestimate of our measured k_2(298 K). Therefore, the quoted rate coefficient for the reaction of Cl + *p*-$ClC_6H_4CF_3$ should be considered an upper limit.

Table 5. Summary of experimental conditions and obtained rate coefficient results in this work for the Cl + *p*-$ClC_6H_4CF_3$ (para-chlorobenzotrifluoride, PCBTF) gas-phase reaction at 298 K using a relative rate method with Cl + CH_3CCl_3 as the reference reaction

$[PCBTF]_0$ (10^{13} molecule cm^{-3})	$[CH_3CCl_3]_0$ (10^{13} molecule cm^{-3})	PCBTF-H_3O^+ (m/z: 161) [a]	PCBTF-NO^+ (m/z: 210) [a]	PCBTF-O_2^+ (m/z: 180) [a]	Average k_{PCBTF}/k_{Ref} [b]	k_{PCBTF} (10^{-16} cm^3 molecule^{-1} s^{-1}) [c]
8.82	1.19	0.086 ± 0.003	0.084 ± 0.006	0.091 ± 0.007	0.087 ± 0.011	7.83 ± 1.57
8.82	2.35	0.088 ± 0.002	0.093 ± 0.002	0.078 ± 0.010	0.086 ± 0.009	7.74 ± 1.45
17.6	11.8	0.092 ± 0.004	0.086 ± 0.003	0.087 ± 0.003	0.088 ± 0.008	7.92 ± 1.43

[a] Uncertainties are 2σ fit precision; [b] Cl + CH_3CCl_3 reference reaction with k_{Ref}(298 K) = (9.0 ± 1.4) × 10^{-15} cm^3 molecule^{-1} s^{-1};[23] [c] 2σ uncertainties that include estimated systematic error.

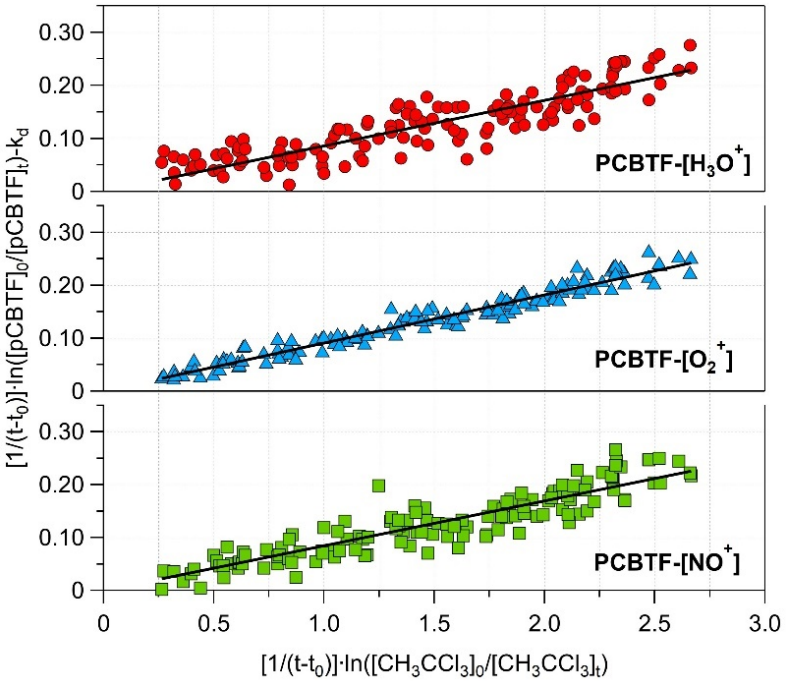

Figure 6. Relative rate determination for the reaction of Cl + PCBTF (*p*-$ClC_6H_4CF_3$) at 298 K and 760 Torr. The panels represent different ion induced chemistry as labeled. The Cl + CH_3CCl_3 reaction was used as the reference reaction.

The Cl atom reactivity towards PCBTF was measured to be at least ~200 times lower compared to the OH radical reaction rate coefficient. Although this observation is not typical for non-aromatic compounds, it is not uncommon in reactions that proceed with aromaticity breaking, e.g., the Cl + C_6H_6 reaction. To the best of our knowledge, there are no previous measurements of k_2 to compare with the present results. A comparison of the Cl + PCBTF rate coefficient with several other Cl + aromatic compounds is presented in **Table 6**. The results from this work are consistent with the limited available data. In addition, it can be seen that the chloro-substitution of benzene reduces the reactivity with Cl atoms. Additional substitution with a -CF_3 group, in the case of

chloro-benzene, is expected to further decrease the Cl reactivity. It is worthwhile to note, that although the halo-substitution of benzene decreases the chemical reactivity of the aromatic compound towards Cl atoms, that is not the case when an OH group is attached to the ring. Cl atom reaction with phenol is about five orders of magnitude greater compared to benzene, indicating that an H-abstraction channel that is not directly breaking the aromaticity of the compound is activated, which substantially reduces the energy barrier for the reaction.

Table 6. Comparison of Cl + aromatic compound rate coefficients at 298 K

Compound	k(298 K) (cm^3 $molecule^{-1}$ s^{-1})	Reference
C_6H_6	$(1.3 \pm 1.0) \times 10^{-16}$	Sokolov at al.[38]
C_6H_5Cl	$<2.5 \times 10^{-16}$	Sokolov et al.[38]
C_6H_5OH	$(1.93 \pm 0.25) \times 10^{-10}$	Jenkin et al. [39]
$ClC_6H_4CF_3$	$(0.78 \pm 0.16) \times 10^{-15}$	This Work

OH and Cl + PCBTF Reaction Mechanisms

The reaction mechanism for the oxidation of PCBTF via OH radical addition has four different reaction pathways, while the direct abstraction or H_2O elimination adds two additional reaction channels as shown in **Figure 7**.[40] A simplified scheme for the Cl + PCBTF reaction is shown in **Figure S9**.

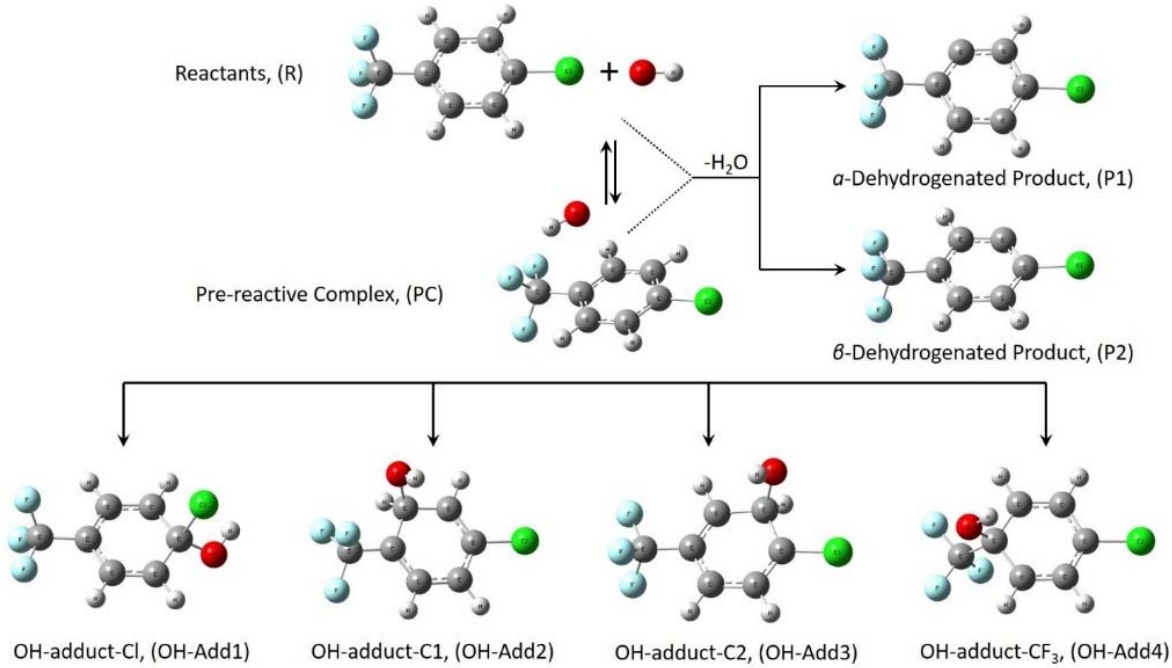

Figure 7. Simplified mechanistic scheme for the OH reaction with PCBTF (*p*-$ClC_6H_4CF_3$). Structures were optimized at the M06-HF/TZVP level of theory.

The kinetic data from this work revealed $k_1(T)$ to have a negative temperature dependence in the low-temperature regime, which is consistent with the formation of a semi-stable OH-PCBTF adduct. At temperatures greater than 450 K, a positive temperature dependence was observed, i.e., the rate coefficient increases with increasing temperature. Our thermochemical calculations indicate that the OH reaction proceeds initially via a pre-reactive complex formation that is exothermic by ≅ -3 kJ mol^{-1}, see **Figure 8**. OH radicals approach the center of the aromatic ring at an angle, allowing its stabilization via electrostatic interactions between $^{\delta-}O\text{-}H^{\delta+}$ … $^{\delta-}F\text{-}C^{\delta+}$. In this formation, the distance between the oxygen atom of the hydroxyl radical and the $C(CF_3)$ carbon of the six-member ring, the α- and β-thesis carbon with respect $C(CF_3)$, are ~2.8, 2.7 and 3.2 Å, respectively. The distance between the oxygen atom of the OH radical and the C(Cl) carbon is much longer, ~3.8 Å. The stabilization of the system is enhanced due to the pre-reactive complex formation and subsequently favors the OH-adduct formation. For all four OH-adducts, the high exothermicity of the reaction limits adduct decomposition back to reactants at temperatures below ~298 K.

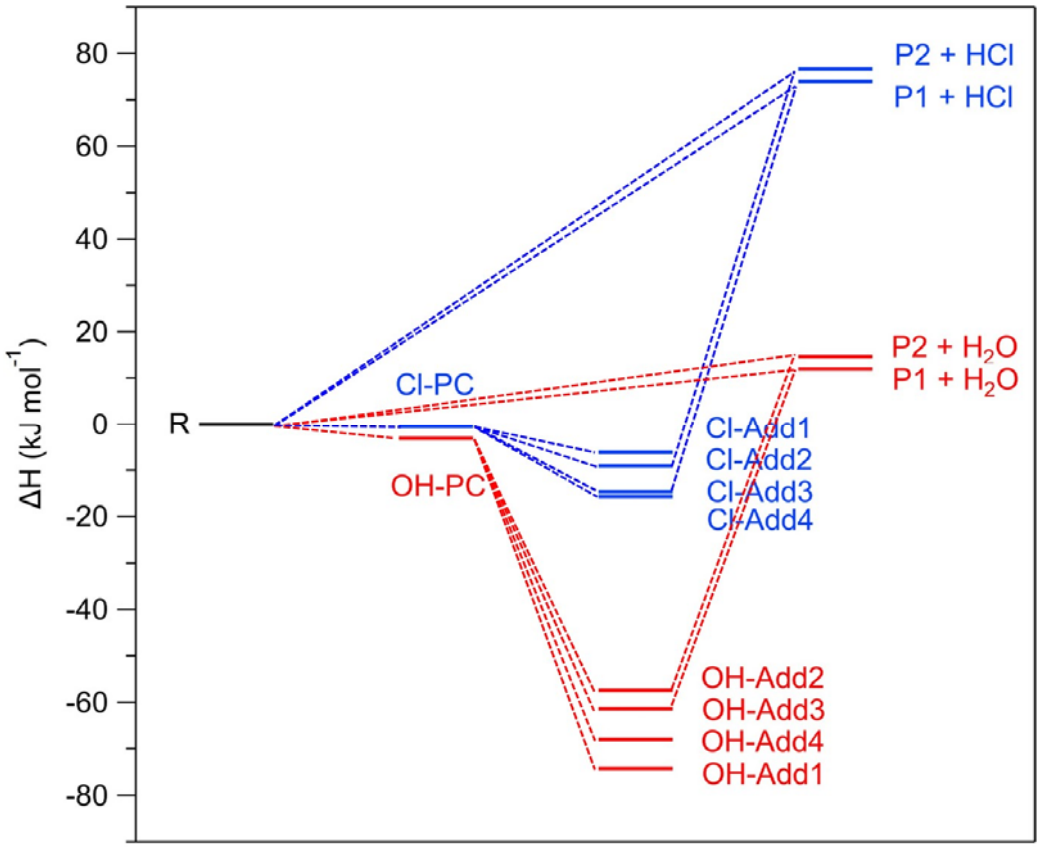

Figure 8. Calculated reaction enthalpies (CCSD(full)/TZVP//M06-HF/TZVP) for the R (OH and Cl) association reactions with PCBTF, proceeding, initially, via a semi-stable pre-reactive complex, OH-PC and Cl-PC, followed by semi-stable adducts formation, OH-add# and Cl-add#, with numbering based on **Figure 7** and **Figure S9**. OH adduct formation channels are highly exothermic, with the most stable adduct being OH addition to C(CCl) carbon (OH-Add1), $\Delta H_r \cong$ -74 kJ mol^{-1}, followed by the one with OH attaching the C(CF_3) carbon, $\Delta H_r \cong$ -68 kJ mol^{-1}. *α*- (OH-Add2) and *β*-thesis (OH-Add3) addition channels are about -57 and -61 kJ mol^{-1} exothermic, respectively. Cl-adduct reaction pathways are slightly exothermic by 6 – 16 kJ mol^{-1}. H-atom direct abstraction channels, OH-P# + H_2O and Cl-P# + HCl are endothermic by ~ +15 and 75 kJ mol^{-1}, respectively.

The theoretical calculations show that the most thermodynamically favorable addition channels are at the C(Cl), $\Delta H_r \cong$ -74 kJ mol^{-1}, and C(CF_3), $\Delta H_r \cong$ -68 kJ mol^{-1}, carbons of the ring, while the *m*- and *o*-thesis, with respect the C(CF_3), lead to adduct-formation channels that are about -61, and -57 kJ mol^{-1} exothermic, respectively. Although activation barriers have not been calculated in the present work, it is expected that the OH-addition to the carbon connected with the bulky -Cl and -CF_3 groups will be less kinetically favorable, mainly due to steric effects. On the other hand, assuming that the OH addition to *o*- and *m*-thesis have similar barriers, OH-Add3 is thermodynamically preferable by ~4 kJ mol^{-1} and would be the most energetically favorable reaction channel. The latter is consistent with the observation of Young et al.[11] that 2-chloro-5-trifluoromethylphenol (*o*-CTFP) is an end-product formed via OH addition followed by either a

hydrogen-shift or hydrogen abstraction by O_2 to form HO_2 that stabilizes the system via regaining its aromaticity. The present results are also consistent with the Lauraguais et al.[41] and Wei et al.[42] studies in which they determined the reactivity trends of a series of aromatics with the NO_3 radical using natural population analysis to calculate the electron density. Their work concluded that the addition of electron withdrawing groups, such as -CF_3 and -Cl, on the aromatic ring enhances the *m*-thesis electron density, favoring the electrophilic addition at that site. However, -CF_3 is a stronger electron withdrawing functional group and thus the *m*-thesis with regard the C(CF_3) carbon would be expected to be the preferred reaction site. However, there might be various other reaction pathways that will lead to the same end-product, following the initial OH radical addition to *o*- or *m*-carbons and the subsequent reaction with O_2. It is also worth mentioning that if OH adds to the C(Cl) carbon, it is very likely for the system to eliminate the Cl atom and form the α,α,α-trifluoro-*p*-cresol. Once the OH-adducts have been formed, in all cases, it is highly unlikely for the system to undergo a four-center H_2O elimination at temperatures <~500 K, since these channels are at least by ~70 kJ mol^{-1} endothermic and would not compete with the reaction of the adducts with O_2. The atmospheric oxidation of PCBTF is complex and quantitative measurements of the stable end-products is desired.

In an attempt to estimate the thermal stability of the formed adducts, the free energy for every single reaction channel was also calculated as a function of temperature. *o*- and *m*- adduct-formation channels have positive ΔG_r values at temperatures around and above 440 and 500 K, respectively, which is consistent with the experimental observations of a mechanism-change in this temperature regime. As far as Cl chemistry is concerned, the rate coefficient for the Cl-atom reaction with PCBTF is significantly lower, three order of magnitude, than the one for the OH radical. Contrary to the OH reaction, although there are no significant electrostatic interactions between Cl atom and the functional groups attached in the aromatic ring of PCBTF that enhance its stability, the Cl pre-reactive complex formation channel (**Figure 8**) is still active ($\Delta H_r \cong$ -1 kJ mol^{-1}), mainly due to the high electron affinity of Cl atoms,[43] and their increased polarizability, compared to the OH radical. However, the *o*- and *m*- Cl-adduct formation channels are almost thermoneutral. Although barrier heights are currently unknown, it is likely that this prohibits the aromatic system from breaking its conjugation, since it would lead to system destabilization (high activation barrier) and, most likely, the Cl pre-reactive complex, thermodynamically driven, will dissociate back to reactants. Note that Cl-adduct formation pathways were calculated to be

exothermic by less than ~16 kJ mol^{-1} compared to the ~ 60 kJ mol^{-1} for the OH reactions implying that if formed they can readily decompose back to the initial reactants, even at room temperature. Therefore, the endothermic (≅ +75 kJ mol^{-1}), direct abstraction reaction channels, with high kinetic barriers are expected to dominate the reaction mechanism, which explains the Cl atom low reactivity towards PCBTF and aromatic compounds in general.

UV absorption spectrum. The PCBTF UV absorption spectrum that was measured using Zn lamp and CCD setups is shown in **Figure 9** and given in **Table S1** at 0.5 nm intervals. The CCD and Zn atomic line cross section measurements agreed to within 5% with σ_{Zn}(213.9 nm) = (3.02 ± 0.07) × 10^{-17} cm^2 $molecule^{-1}$ and σ_{CCD}(213.9 nm) = (3.17 ± 0.07) × 10^{-17} cm^2 $molecule^{-1}$, where the quoted uncertainties are the fit precision. An average value of 3.1 × 10^{-17} cm^2 $molecule^{-1}$ is recommended and was used to normalize the CCD spectrum shown in **Figure 9** and the data in **Table S1**. Over the 200 to 350 nm range of the PCBTF spectrum, there are clearly multiple electronic transitions active with a strong maximum near 216 nm, a weaker band with a peak near 260 nm that shows diffuse band structure, and a broad absorption with a weak maximum near 300 nm that falls in the solar actinic region for the troposphere.

The absolute uncertainty in the PCBTF UV cross sections was estimated from the precision of the sample preparation and the accuracy of the absorption measurements to be ~5% over the 280 to 320 nm region and ~10% in the 280 to 320 nm region, with an increasing uncertainty toward longer wavelengths, up to ~100% at 350 nm. Atkinson et al.[10] reported a PCBTF UV absorption spectrum graphically between 230 and 300 nm. Although reliable data is most likely only available for wavelengths less than 280 nm in their study, the spectrum is in general agreement with the present work.

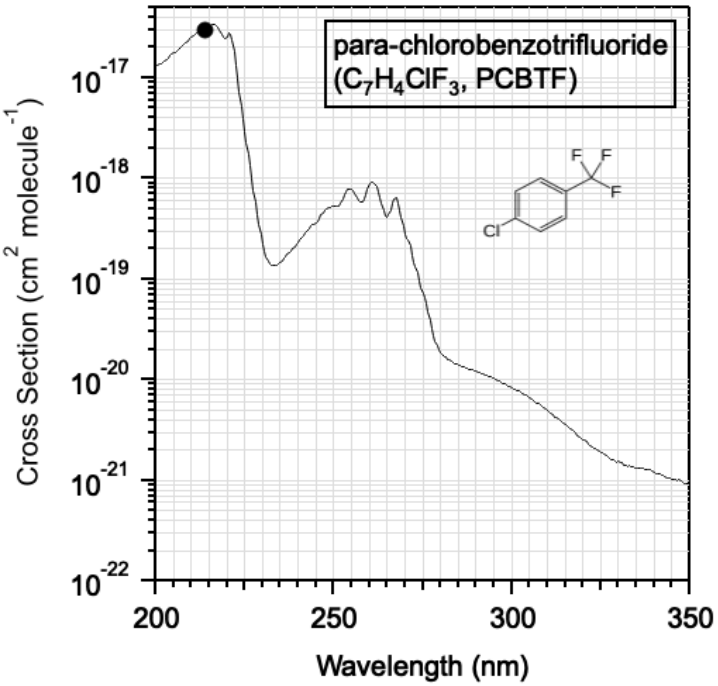

Figure 9. Gas-phase 298 K UV absorption spectrum of para-chlorobenzotrifluoride (*p*-$ClC_6H_4CF_3$, PCBTF) measured in this work using a CCD spectrometer (~1 nm resolution) (see text). Recommended cross section data are provided in **Table S1**. The solid circle is the absorption cross section measured in this work at the Zn 213.9 nm atomic line (see text).

PCBTF absorbs in the tropospheric actinic region, wavelengths greater than 295 nm, and photolysis is an atmospheric loss process that requires consideration. A representative photolysis rate coefficient, *J*, calculation for ground level photolysis in the Northern mid-latitudes in July yields an instantaneous photolysis lifetime of ~3-4 days. Note that photolysis quantum yield studies for PCBTF are currently not available and this calculation assumes a photolysis quantum yield of unity. Therefore, this *J* value represents an upper-limit for the photolysis loss rate of PCBTF. Using black light irradiation, Atkinson et al.[10] report a PCBTF photolysis lifetime to be >6.5 days. The atmospheric lifetime of PCBTF due to reactive loss with the OH radical is estimated to be ~70 days, based on the kinetic results from this work. Clearly, further studies that quantify the UV photolysis of PCBTF are needed to better establish the overall atmospheric lifetime of PCBTF.

Infrared absorption spectrum. The PCBTF infrared absorption spectrum measured in this work is shown in **Figure 10** and a digitized spectrum is provided in the SI. Absorption cross sections were measured using Beer's law. The integrated band strength over the 700–1700 cm^{-1} region was determined to be 1.61×10^{-16} cm^2 $molecule^{-1}$ cm^{-1}, with a measurement precision of

~5%. The peak cross section for the strongest band in this region at 1329.4 cm^{-1} was measured to be 3.04×10^{-18} cm^2 $molecule^{-1}$.

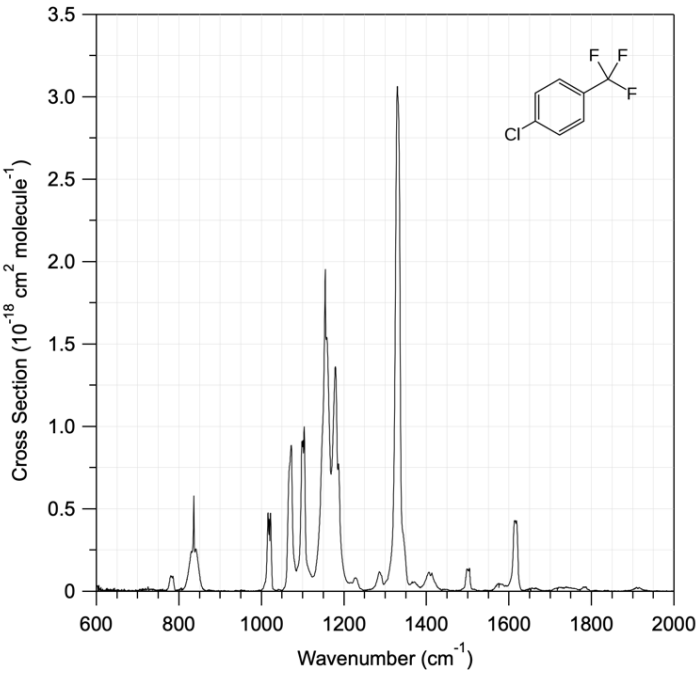

Figure 10. Gas-phase 298 K infrared absorption spectrum of para-chlorobenzotrifluoride (*p*-$ClC_6H_4CF_3$, PCBTF) measured in this work using a Fourier transform spectrometer at 0.5 cm^{-1} resolution. A digitized PCBTF spectrum is provided in the SI.

Conclusions

In this study, rate coefficients for the OH radical (275–940 K, 4–760 Torr) and Cl atom (296 K, 760 Torr) reaction with PCBTF was measured experimentally using a combination of complementary absolute and relative rate methods. The kinetic data measured in this study are suitable to be used in photochemical atmospheric modelling. Quantum mechanical molecular calculations (CCSD(full)/TZVP//M06-HF/TZVP) were also used to look into the degradation mechanism of PCBTF and compared with kinetic data available for other aromatic compounds.

Reaction mechanism of a substituted aromatic compound. The observed trends of the OH + PCBTF reaction temperature dependent rate coefficient is evidence for a change in the reaction mechanism with H-atom abstraction and adduct formation channels dominating at temperatures > 450 K and < 400 K, respectively. At atmospherically relevant temperatures, <298 K, a negative activation energy war measured, which is consistent with an association reaction mechanism. At

higher temperatures, the OH-PCBTF adduct formation channels become thermodynamically less favorable, which primarily accounts for the "dip" in the observed OH reactivity above 400 K. Our quantum mechanical calculations revealed that the OH reaction with PCBTF proceeds predominantly via a pre-reactive complex formation leading to intermediate semi-stable adduct products. A comprehensive theoretical analysis of the temperature and pressure dependence of the phenomenological rate coefficient for the OH + PCBTF reaction is ongoing in our laboratory and will be the subject of a future publication.

Although, a pre-reactive complex formation channel was also calculated for the Cl + PCBTF reaction, the Cl-adduct products stability is substantially lower, leading to almost thermoneutral reaction channels. The latter accounts, for the most part, for the substantially lower measured Cl atom reactivity. This also explains, in part, the substantially lower reaction rate coefficients for the addition of the Cl atom to many other substituted aromatic compounds. In general, for substituted aromatics containing H-donors, where the Cl reaction proceeds via a direct H-atom abstraction, the Cl reactivity is substantially enhanced leading to reaction rate coefficients greater than for the analogous OH radical reaction. Our theoretical calculations revealed that the OH-adduct formation channels are significantly more exothermic compared to the Cl association reactions. The stability of the OH-PCBTF adducts minimizes the adduct decomposition back to reactants resulting in greater effective OH rate coefficients compared with the Cl reaction.

Atmospheric Implications. Potential atmospheric removal processes of PCBTF include the reaction with OH and NO_3 radicals, O_3 and Cl atoms as well as UV photolysis. In this work, the rate coefficient for the OH + PCBTF gas-phase reaction was measured for conditions most relevant to the troposphere, where the reaction is at its high-pressure limit with a negative temperature dependence. The rate coefficient is well described by the Arrhenius expression $k_1(275–385\ K) = (1.50 \pm 0.15) \times 10^{-14} \exp((705 \pm 30)/T)$ cm^3 molecule^{-1} s^{-1}. The present results are ~30% lower than the previously reported k(298 K) values of Atkinson et al.[10] and Young et al.[11] On the basis of the present work, the atmospheric lifetime of PCBTF with respect to reaction with the OH radical is estimated to be ~70 days. Atkinson et al. reported a room temperature rate coefficient for the O_3 + PCBTF reaction to be $<5 \times 10^{-21}$ cm^3 molecule^{-1} s^{-1}. Our work has shown the rate coefficient for the Cl + PCBTF reaction to be $(7.8 \pm 2) \times 10^{-16}$ cm^3 molecule^{-1} s^{-1}. Given the globally averaged background levels of atmospheric O_3 and Cl atoms, 10^{12} and 10^4 molecule cm^{-3}, respectively, neither of these reactions represent a significant PCBTF loss process. There is not kinetic data

currently available for the reaction of PCBTF with NO_3 radicals, however, it is not expected to contribute to the overall atmospheric loss of PCBTF.[41,42]

Although PCBTF is a relatively weak UV absorber at wavelengths greater than 295 nm, assuming a PCBTF photolysis quantum yield of unity at all wavelengths, the mid-day instantaneous PCBTF photolysis lifetime at ground level mid-latitudes is estimated to be ~3–4 days. It is highly likely that the PCBTF photolysis quantum yield at wavelengths greater than 300 nm is, however, not unity. Further research is required to quantify the UV photolysis loss process.

On the basis of the present work, the radiative efficiency (RE) and global warming potential (GWP) of PCBTF were estimated. Using the Shine and Myhre[44] irradiance profile that includes a molecule dependent stratospheric temperature adjustment, the atmospherically well-mixed RE for PCBTF is 0.22 W m^{-2} ppb^{-1}. Using the low-frequency absorption and lifetime adjustment factors of 1.033 and 0.387, respectively, yields an adjusted RE of 0.088 W m^{-2} ppb^{-1}. Using the 2019 CO_2 level 100-year time horizon absolute GWP (AGWP) of 8.947×10^{-14} W yr/(m^2 kg), the 100-year time horizon GWP for PCBTF is 5.9.

Although there is limited kinetic and degradation information available for substituted aromatic compounds, we have estimated the Photochemical Ozone Creation Potential ($POCP_E$) for PCBTF. As interpreted from measurements of PCBTF in urban environments,[9] PCBTF was thought to potentially impact ozone production on a local to regional scale. The $POCP_E$ was estimated using the expression given in Jenkin et al.[45] that was based on the MCM v3.1 idealized box model for a limited number of aromatics. The calculated $POCP_E$ upper limit for PCBTF was found to be relatively small, <2. Based solely on the OH radical reactive loss of PCBTF, this would imply that PCBTF has a minor impact on ozone production on the local urban spatial scale.

ASSOCIATED CONTENT

Supporting Information

The Supporting Information is available free of charge on the ACS Publications website at DOI: xxxx.

Figure S1 and S2. Low- and high-temperature flow reactor diagrams; **Figure S3.** Representative OH temporal profiles, at 645 K; **Figure S4.** Temperature dependent pseudo first-order OH rate coefficient; **Figure S5.** Relative rate measurement for the reaction of OH + PCBTF at 325 K and 760 Torr; **Figure S6.** Relative rate measurement for the reaction of OH + PCBTF at 353 K and 760 Torr; **Figure S7 and S8.** Relative rate measurement for the reaction of Cl + PCBTF at 298 K and 760 Torr; **Figure S9.** Simplified mechanistic scheme for the Cl + PCBTF reaction; **Table S1.** Measured UV cross-section data for PCBTF, between 200 – 350 nm, at 298 K; **Separate File.** Digitized infrared absorption spectrum for PCBTF (JCAMP)

AUTHOR INFORMATION

Notes

The authors declare no competing financial interest.

Acknowledgements

The work at NOAA was supported in part by the NOAA Climate Goal and NASA Atmospheric Composition Programs. ADE was co-funded by the Erasmus+ programme of the European Union for visiting IMT Nord Europe institute. This work is part of the CaPPA project funded by the ANR through the PIA under contract ANR-11-LABX-0005-01, the “Hauts-de-France” Regional Council and the European Regional Development Fund (ERDF). VCP was supported in part by Labex CaPPA, IMT Nord Europe.

REFERENCES

(1) Calvert, J. G.; Atkinson, R.; Becker, K. H.; Kamens, R. M.; Seinfeld, J. H.; Wallington, T. J.; Yarwood, G. *The Mechanisms of Atmospheric Oxidation of Aromatic Hydrocarbons*; Oxford University Press: New York, 2002.

(2) Thiault, G.; Mellouki, A.; Le Bras, G. Kinetics of gas phase reactions of OH and Cl with aromatic aldehydes. *Phys. Chem. Chem. Phys.* **2002**, *4*, 2194–2199.

(3) Thüner, L. P.; Bardini, P.; Rea, G. J.; Wenger, J. C. Kinetics of the gas-phase reactions of OH and NO_3 radicals with dimethylphenols. *J. Phys. Chem. A* **2004**, *108*, 11019−11025.

(4) Seta, T.; Nakajima, M.; Miyoshi, A. High-temperature reactions of OH radicals with benzene and toluene. *J. Phys. Chem. A* **2006**, *110*, 5081-5090.

(5) Kovacevic, G.; Sabljic, A. Atmospheric oxidation of halogenated aromatics: comparative analysis of reaction mechanisms and reaction kinetics. *Environ. Sci.: Processes Impacts* **2017**, *19*, 357–369.

(6) Lu, T.; Huang, M.; Lin, X.; Zhang, W.; Zhao, W.; Hu, C.; Gu, X.; Zhang, W. Theoretical studies on the reaction mechanism and kinetics of ethylbenzene-OH adduct with O_2 and NO_2. *Atmosphere* **2021**, *12*, 1118

(7) Yan Li, X. G.; Zhang, R. M.; Zhang, H.; Zhang, X.; Xu, X. Pressure-dependent kinetics of the o-xylene reaction with OH radicals. *Phys. Chem. Chem. Phys.* **2022**, *24*, 8672–8682.

(8) McDonald, B. C.; de Gouw, J. A.; Gilman, J. B.; Jathar, S. H.; Akherati, A.; Cappa, C. D.; Jimenez, J. L.; Lee-Taylor, J.; Hayes, P. L.; McKeen, S. A.; et al. Volatile chemical products emerging as largest petrochemical source of urban organic emissions. *Science* **2018**, *359*, 760-764.

(9) Gkatzelis, G. I.; Coggon, M. M.; McDonald, B. C.; Peischl, J.; Aikin, K. C.; Gilman, J. B.; Trainer, M.; Warneke, C. Identifying volatile chemical product tracer compounds in U.S. cities. *Environ. Sci. Tech.* **2021**, *55*, 188-199.

(10) Atkinson, R.; Aschmann, S. M.; Winer, A. M.; Pitts, J. N. Atmospheric gas phase loss processes for chlorobenzene, benzotrifluoride, and 4-chlorobenzotrifluoride, and generalization of predictive techniques for atmospheric lifetimes of aromatic compounds. *Archives Environm. Contami. Tox.* **1985**, *14*, 417-425.

(11) Young, C. J.; Gómez Biagi, R. F.; Hurley, M. D.; Wallington, T. J.; Mabury, S. A. Paint solvent to food additive: An environmental route of dehalgenation for 4-chlorobenzotrifluoride. *Environ. Tox. Chem.* **2008**, *27*, 2233-2238.

(12) Bedjanian, Y. Temperature-dependent rate constant for the reaction of hydroxyl radical with 3-hydroxy-3-methyl-2-butanone. *J. Phys. Chem. A* **2019**, *123*, 10446-10453.

(13) Bedjanian, Y.; Morin, J.; Romanias, M. N. Reactions of OH radicals with 2-methyl-1-butyl, neopentyl and 1-hexyl nitrates. Structure-activity relationship for gas-phase reactions of OH with alkyl nitrates: An update. *Atmos. Environ.* **2018**, *180*, 167-172.

(14) Morin, J.; Romanias, M. N.; Bedjanian, Y. Experimental study of the reactions of OH radicals with propane, n-pentane, and n-heptane over a wide temperature range. *Int. J. Chem. Kinet.* **2015**, *47*, 629-637.

(15) Bedjanian, Y. Rate constants of the reaction of OH radicals with HBr over the temperature range 235-960 K *J. Phys. Chem. A* **2021**, *125*, 1754-1759.

(16) Kaufman, F. Kinetics of elementary radical reactions in the gas phase. *J. Phys. Chem.* **1984**, *88*, 4909-4917.

(17) Ivanov, A. V.; Trakhtenberg, S.; Bertram, A. K.; Gershenzon, Y. M.; Molina, M. J. OH, HO_2, and ozone gaseous diffusion coefficients. *J. Phys. Chem. A* **2007**, *111*, 1632-1637.

(18) Su, M. C.; Kumaran, S. S.; Lim, K. P.; Michael, J. V.; Wagner, A. F.; Harding, L. B.; Fang, D. C. Rate constants, 1100 ≤ T ≤ 2000 K, for H + NO_2 → OH + NO using two shock tube techniques: Comparison of theory to experiment. *J. Phys. Chem. A* **2002**, *106*, 8261-8270.
(19) Bedjanian, Y.; Le Bras, G.; Poulet, G. Kinetic study of the reactions of Br_2 with OH and OD. *Int. J. Chem. Kinet.* **1999**, *31*, 698-704.
(20) Bedjanian, Y.; Le Bras, G.; Poulet, G. Kinetic study of OH + OH and OD + OD reactions. *J. Phys. Chem. A* **1999**, *103*, 7017-7025.
(21) Osseiran, N.; Romanias, M. N.; Gaudion, V.; Angelaki, M. E.; Papadimitriou, V. C.; Tomas, A.; Coddeville, P.; Thevenet, F. Development and validation of a thermally regulated atmospheric simulation chamber (THALAMOS): A versatile tool to simulate atmospheric processes. *J. Environ. Sci.* **2020**, *95*, 141-154.
(22) Allani, A.; Bedjanian, Y.; Papanastasiou, D. K.; Romanias, M. N. Reaction Rate coefficient of OH radicals with d_9-butanol as a function of temperature. *ACS Omega* **2021**, *28*, 18123–18134.
(23) Burkholder, J. B.; Sander, S. P.; Abbatt, J.; Barker, J. R.; Cappa, C.; Crounse, J. D.; Dibble, T. S.; Huie, R. E.; Kolb, C. E.; Kurylo, M. J.; et al. "Chemical Kinetics and Photochemical Data for Use in Atmospheric Studies, Evaluation No. 19," JPL Publication 19-5, Jet Propulsion Laboratory, Pasadena, 2020 http://jpldataeval.jpl.nasa.gov. **2020**.
(24) Smith, D.; Spanel, P. Selected ion flow tube mass spectrometry (SIFT-MS) for on-line trace gas analysis. *Mass Spec. Rev.* **2005**, *24*, 661-700.
(25) Zhao, Y.; Truhlar, D. G. Comparative DFT study of van der Waals complexes: Rare-gas dimers, alkaline-Earth dimers, zinc dimer, and zinc-rare-gas dimers. *J. Phys. Chem. A* **2006**, *110*, 5121-5129.
(26) Zhao, Y.; Truhlar, D. G. Density functional for spectroscopy: No long-range self-interaction error, good performance for rydberg and charge-transfer states, and better performance on average than B3LYP for ground states. *J. Phys. Chem. A* **2006**, *110*, 13126-13130.
(27) Schäfer, A.; Horn, H.; Ahlrichs, R. Fully optimized contracted Gaussian basis sets for atoms Li to Kr. *J. Chem. Phys.* **1992**, *97*, 2571-2577.
(28) Schäfer, A.; Huber, C.; Ahlrichs, R. Fully optimized contracted Gaussian basis sets of triple zeta valence quality for atoms Li to Kr. *J. Chem. Phys.* **1994**, *100*, 5829-5835.
(29) Čížek, J. On the use of the cluster expansion and the technique of diagrams in calculations of correlation effects in atoms and molecules. *Adv. Chem. Phys.* **1969**, 35-89.
(30) Purvis, G. D., III; Bartlett, R. J. A full coupled-cluster singles and doubles model: The inclusion of disconnected triples. *J. Chem. Phys.* **1982**, *76*, 1910-1918.
(31) Scuseria, G. E.; Janssen, C. L.; Schaefer, H. F., III An efficient reformulation of the closed-shell coupled cluster single and double excitation (CCSD) equations. *J. Chem. Phys.* **1988**, *89*, 7382-7387.
(32) Scuseria, G. E.; Schaefer, H. F., III Is coupled cluster singles and doubles (CCSD) more computationally intensive than quadratic configuration interaction (QCISD)? *J. Chem. Phys.* **1989**, *90*, 3700-3703.
(33) Zhao, Y.; Truhlar, D. G. The M06 suite of density functionals for main group thermochemistry, thermochemical kinetics, noncovalent interactions, excited states, and transition elements: two new functionals and systematic testing of four M06-class functionals and 12 other functionals. *Theor. Chem. Account.* **2008**, *120*, 215–241.
(34) Zhao, Y.; Truhlar, D. G. The M06 suite of density functionals for main group thermochemistry, thermochemical kinetics, noncovalent interactions, excited states, and transition

elements: two new functionals and systematic testing of four M06 functionals and 12 other functionals. *Theor. Chem. Account.* **2008**, *119*, 525.
(35) Zhao, Y.; Truhlar, D. G. Density functionals with broad applicability in chemistry. *Acc. Chem. Res.* **2008**, *41*, 157–167.
(36) M. J. Frisch; G.W.T.; Schlegel, H. B.; Scuseria, G. E.; Robb, M. A.; Cheeseman, J. R.; Scalmani, G.; Barone, V.; Mennucci, B.; Petersson, G. A.; et al. Gaussian09, Gaussian Inc.: Wallingford CT. **2013**.
(37) "NIST Chemical Kinetics Database, NIST Standard Reference Database 17, Version 7.0 (Web Version)", https://kinetics.nist.gov/, Release 1.6.8, Data version 2015.09, Accesed 2022.06.
(38) Sokolov, O.; Hurley, M. D.; Wallington, T. J.; Kaiser, E. W.; Platz, J.; Nielsen, O. J.; Berho, F.; Rayez, M.-T.; Lesclaux, R. Kinetics and mechanism of the gas-phase reaction of Cl Atoms with benzene. *J. Phys. Chem. A* **1998**, *102*, 10671–10681.
(39) Jenkin, M. E.; Hurley, M. D.; Wallington, T. J. Investigation of the radical product channel of the $CH_3OCH_2O_2$ + HO_2 reaction in the gas phase. *J. Phys. Chem. A* **2010**, *114*, 408-416.
(40) Atkinson, R. Kinetics and mechanisms of the gas-phase reactions of the hydroxyl radical with organic compounds. *J. Phys. Chem. Ref. Data* **1989**, *Monograph 1*, 246p.
(41) Lauraguais, A. l.; El Zein, A.; Coeur, C.; Obeid, E.; Cassez, A.; Rayez, M. T.; Rayez, J.-C. Kinetic study of the gas-phase reactions of nitrate radicals with methoxyphenol compounds: Experimental and theoretical approaches. *J. Phys. Chem. A* **2016**, *120*, 2691−2699.
(42) Wei, B.; Sun, J.; Mei, Q.; An, Z.; Cao, H.; Han, D.; Xie, J.; Zhan, J.; Zhang, Q.; Wang, W.; et al. Reactivity of aromatic contaminants towards nitrate radical in tropospheric gas and aqueous phase. *J. Hazard. Mater.* **2021**, *401*, 123396.
(43) Smith, I. W. M.; Ravishankara, A. R. Role of Hydrogen-Bonded Intermediates in the Bimolecular Reactions of the Hydroxyl Radical. *J. Phys. Chem. A* **2002**, *106*, 4798-4807.
(44) Shine, K. P.; Myhre, G. The spectral nature of stratospheric temperature adjustment and its application to halocarbon radiative forcing. *J. Adv. Mod. Earth Sys.* **2020**, *12*, 16.
(45) Jenkin, M. E.; Derwent, R. G.; Wallington, T. J. Photochemical ozone creation potentials for volatile organic compounds: Rationalization and estimation. *Atmos. Environ.* **2017**, *163*, 128-137.

TOC Image

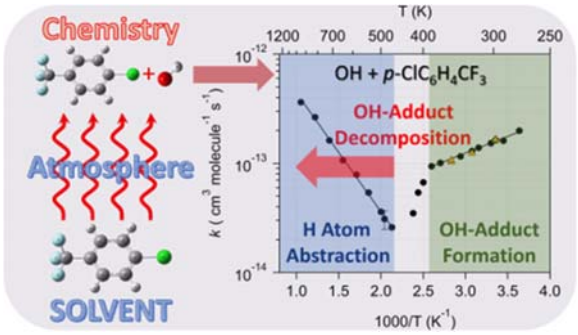
Chemistry
Atmosphere
SOLVENT
T (K)
1200 700 500 400 300 250
OH + p-ClC6H4CF3
OH-Adduct
Decomposition
H Atom
Abstraction
OH-Adduct
Formation
k (cm3 molecule-1 s-1)
10-12
10-13
10-14
1.0 1.5 2.0 2.5 3.0 3.5 4.0
1000/T (K-1)